



HAL
open science

Growth and Characterization of Yb: CALYGLO Crystal for Ultrashort Pulse Laser Applications

Zebin Wang, Jian Liu, Peng Chen, Peng Liu, Jie Ma, Xiaodong Xu, Yong Wei, Kheirreddine Lebbou, Jun Xu

► **To cite this version:**

Zebin Wang, Jian Liu, Peng Chen, Peng Liu, Jie Ma, et al.. Growth and Characterization of Yb: CALYGLO Crystal for Ultrashort Pulse Laser Applications. *Crystals*, 2024, 14 (2), pp.120. 10.3390/cryst14020120 . hal-04499932

HAL Id: hal-04499932

<https://hal.science/hal-04499932>


Submitted on 11 Mar 2024

HAL is a multi-disciplinary open access archive for the deposit and dissemination of scientific research documents, whether they are published or not. The documents may come from teaching and research institutions in France or abroad, or from public or private research centers.

L'archive ouverte pluridisciplinaire **HAL**, est destinée au dépôt et à la diffusion de documents scientifiques de niveau recherche, publiés ou non, émanant des établissements d'enseignement et de recherche français ou étrangers, des laboratoires publics ou privés.

Article

Growth and Characterization of Yb: CALYGLO Crystal for Ultrashort Pulse Laser Applications

Zebin Wang ¹, Jian Liu ¹, Peng Chen ², Peng Liu ¹, Jie Ma ¹, Xiaodong Xu ^{1,*}, Yong Wei ³, Kheirredine Lebbou ² 
and Jun Xu ^{4,*}

¹ Jiangsu Key Laboratory of Advanced Laser Materials and Devices, School of Physics and Electronic Engineering, Jiangsu Normal University, Xuzhou 221116, China; jianliu586@jsnu.edu.cn (J.L.)

² Institut Lumière Matière, UMR5306 Université Lyon1-CNRS, Université de Lyon, 69622 Lyon, Villeurbanne Cedex, France; kheirredine.lebbou@univ-lyon1.fr (K.L.)

³ School of Physics and Electronics Science, Hunan Institute of Science and Technology, Yueyang 414006, China

⁴ School of Physics Science and Engineering, Institute for Advanced Study, Tongji University, Shanghai 200092, China

* Correspondence: xdxu79@jsnu.edu.cn (X.X.); 15503@tongji.edu.cn (J.X.)

Abstract: Yb:CALYGLO crystals with a dopant concentration of 5 at.% were successfully grown using the Czochralski method. The crystal samples were extensively studied to analyze their structure, room temperature and low temperature spectra, and laser properties. The highest absorption cross-section at 977 nm was calculated to be 1.83×10^{-20} cm² for σ polarization and 5.32×10^{-20} cm² for π polarization. Similarly, the emission cross-section was determined to be 1.38×10^{-20} cm² at 980 nm for σ polarization and 2.28×10^{-20} cm² at 981 nm for π polarization, with a full width at half maximum (FWHM) of 50.3 nm and 89.5 nm, respectively. The fluorescence lifetime of the 5 at.% Yb:CALYGLO crystal at ²F_{5/2} was measured to be 1.10 ms. Additionally, gain cross-sections were calculated for different β values. In the continuous laser experiment, the crystal demonstrated a laser output of 20.15 W at 1057 nm, with a slope efficiency of 53.3%. These experimental findings indicate that the lattice of Y³⁺ in the crystal is partially replaced by Lu³⁺ and Gd³⁺, resulting in a broader spectrum. Consequently, this crystal shows promising potential as a gain medium for ultrashort pulse laser crystals.



Citation: Wang, Z.; Liu, J.; Chen, P.; Liu, P.; Ma, J.; Xu, X.; Wei, Y.; Lebbou, K.; Xu, J. Growth and Characterization of Yb: CALYGLO Crystal for Ultrashort Pulse Laser Applications. *Crystals* **2024**, *14*, 120. <https://doi.org/10.3390/cryst14020120>

Academic Editor: Lin Gan

Received: 22 December 2023

Revised: 15 January 2024

Accepted: 22 January 2024

Published: 25 January 2024



Copyright: © 2024 by the authors. Licensee MDPI, Basel, Switzerland. This article is an open access article distributed under the terms and conditions of the Creative Commons Attribution (CC BY) license (<https://creativecommons.org/licenses/by/4.0/>).

Keywords: Yb:CALYGLO; Czochralski method; low temperature spectra; ultrafast laser

1. Introduction

The 2023 Nobel Prize in Physics was awarded for a revolutionary method. This method allows the generation of extremely short pulses of light, enabling the precise measurement of rapid electron movements and energy changes. The development of ultrashort pulse lasers has garnered significant interest in various fields including science, industry, medicine, and the military due to their vast potential for application [1–7].

In the near-infrared band, Yb³⁺ ions have simpler energy levels compared to Nd³⁺ ions, consisting of only two manifolds. Furthermore, there are no higher excited state energy levels above the upper level, resulting in the absence of excited state absorption, fluorescence up-conversion, and concentration quenching effects. Additionally, Yb³⁺ doped laser material exhibits a strong absorption band near 940 nm, which can be efficiently pumped by InGaAs LD within the 930–980 nm range, and demonstrates high coupling [8]. Moreover, the large emission bandwidth of Yb³⁺ is advantageous for the generation of ultrashort pulse lasers. Numerous Yb³⁺ doped host materials have been reported in this field, including GdScO₃ [9], YAG [10,11], Y₂O₃ [12], Lu₂O₃ [13], CALGO [14,15], etc.

The CaYAIO₄ crystal belongs to the tetragonal system, and its spatial group is *I4/mmm*. Due to the charge difference and random distribution between Ca²⁺ ions and Y³⁺ ions leading to their disordered lattice structure, the results indicate that the spectral band of

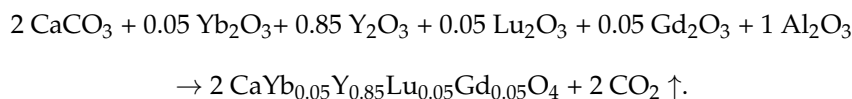
the CaYAlO₄ crystal has obvious uneven broadening [16]. Therefore, when the lattice is doped with Yb³⁺, its absorption and emission spectra will be non-uniformly broadened, which is conducive to the realization of ultrashort pulse laser output. At the same time, the CaYAlO₄ crystal itself is considered as one of the most promising ultrafast laser gain media for commercial development due to its high structural disorder and excellent thermal properties [17]. It has been reported continuously that the shorter pulse laser duration was achieved via the Kerr-lens mode locking (KLM) technique from CaLnAlO₄ lasers [18–21]. It has been reported that the addition of Lu³⁺ ions in CaLnAlO₄ matrix materials increases the disorder of the crystal lattice. The random distribution between Ca²⁺ ions, Y³⁺ (Gd³⁺) ions, and Lu³⁺ ions will further broaden the spectral band of active RE³⁺ doping ions [22,23]. At the same time, in Gd-based oxides, the ionic radii of Lu³⁺ and Yb³⁺ are closer in Lu-based oxides, making doping easier to achieve. Simultaneously, there is a weaker dependence of thermal properties on the doping level. [24]. In recent years, more “mixed” crystals have also been continuously explored [25–27].

In this paper, a single crystal of Yb:CaY_{0.85}Lu_{0.05}Gd_{0.05}AlO₄ with a Yb concentration of 5 at.% was grown using the Czochralski method. The study focused on the growth and structure of the Yb:CALYGLO crystal, as well as the spectral properties of Yb³⁺ in the crystals at room and low temperatures. Additionally, CW laser experiments were conducted on the crystal at room temperature. In CALYO crystals, the substitution of Y³⁺ lattice sites with Lu³⁺ and Gd³⁺ ions was performed to enhance disorder and broaden the spectrum of doped ions, ultimately enabling the generation of ultrashort pulse laser output.

2. Materials and Methods

2.1. Crystal Growth

The 5 at.% Yb:CaY_{0.85}Lu_{0.05}Gd_{0.05}AlO₄ crystal was successfully grown by the Czochralski method. The raw materials were Lu₂O₃, Gd₂O₃, CaCO₃, Al₂O₃, Y₂O₃, Yb₂O₃ powder, with a purity of 99.999%. They were weighed according to the formula:



After the dry powder mixing method was used to achieve uniform mixing, the mixture was then molded into a bar shape and sealed. The bar was cooled under 100 MPa using a cold isostatic pressing machine for 3 min, resulting in a solid block. Subsequently, the block was placed in a muffle furnace and subjected to a presintering process at 1300 °C in an air atmosphere for 20 h. Following this, furnace charging and crystal growth were carried out. CaYAlO₄ crystals with a size of 5 × 5 × 25 mm³ in the crystalline a-axis were used as seed crystals for growth. During the growth process, the pulling rate was 1 mm/h, and the rotation rate was 15 rpm. To prevent the iridium crucible from oxidizing due to the oxygen in the air, a protective atmosphere of high-purity N₂ was used. Once the seed crystal was connected, the power was slightly increased to promote necking, which effectively prevents dislocation and impurities from entering the crystal. After the growth was completed, the crystal was cooled to room temperature for 48 h before being taken out. Finally, the Yb:CALYGLO crystal was obtained, as depicted in Figure 1. The crystal exhibits color centers and appears light yellow, which can be eliminated through annealing.



Figure 1. Photograph of as-grown 5 at.% Yb:CALYGLO crystal.

2.2. X-ray Diffraction and ICP-AES Measurement

The German Bruker D2 type X-ray powder diffractometer was used to perform XRD testing on the Yb:CALYGLO single crystal. Cu-K α radiation was used as the radiation source. The scanning range (2θ) was 5° to 90° , and the step size was 0.01° . The XRD instrument was operated at a setting voltage of 30 kV and a current of 10 mA. The sample used for XRD testing is a small part of the grown Yb:CALYGLO single crystal processed into powder.

In order to understand the segregation of each doping ion in the crystal, inductively coupled plasma atomic emission spectrometry (ICP-AES) was used to measure the Yb:CALYGLO crystal. The plasma emission spectrometer (model: Advantage, Thermo, Manassquan, NJ, USA) used for testing was used to determine the element content. The sample was cut off about 1.0 g from the head of the grown Yb:CALYGLO crystal and then ground into powder for testing. The segregation coefficient can be calculated using Formula (1), and the Yb $^{3+}$ concentration (C_s) in the sample used for spectral measurement can be determined using Formula (2).

$$K_m = \frac{C_t}{C_0} \quad (1)$$

$$C_s = C_0 K_m (1 - g)^{K_m - 1} \quad (2)$$

where C_0 is the concentration of Yb $^{3+}$ when batching; C_t is the concentration of Yb $^{3+}$ at the starting position of crystal growth, g is the crystal crystallization rate, and C_0 is the segregation coefficient. The segregation coefficients of Yb $^{3+}$, Gd $^{3+}$, Lu $^{3+}$, and Y $^{3+}$ were calculated to be 0.65, 0.81, 0.58, and 1.01, respectively. The segregation coefficients of Yb $^{3+}$ and Lu $^{3+}$ ions are similar because they have similar ionic radii, so the difficulty of doping is similar. For Yb $^{3+}$ ions, the calculated result of C_s in the Yb:CALYGLO crystal is 3.4%, and the doping ion concentration per unit volume can be calculated to be $4.34 \times 10^{20} \text{ cm}^{-2}$. The measurement results and calculated segregation coefficients of Yb $^{3+}$, Lu $^{3+}$, Gd $^{3+}$, and Y $^{3+}$ elements in the Yb:CALYGLO crystal are shown in Table 1.

Table 1. The weight proportions and calculated segregation coefficient K of Yb $^{3+}$, Gd $^{3+}$, Lu $^{3+}$, and Y $^{3+}$ in Yb:CALYGLO crystal samples.

5 at.% Yb:CALYGLO Crystal	Measured Yb $^{3+}$ (wt%)	Measured Gd $^{3+}$ (wt%)	Measured Lu $^{3+}$ (wt%)	Measured Y $^{3+}$ (wt%)
	0.90	4.02	1.80	30.69
	K_m of Yb $^{3+}$	K_m of Gd $^{3+}$	K_m of Lu $^{3+}$	K_m of Y $^{3+}$
	0.65	0.81	0.58	1.05

2.3. Spectra Measurements

The samples for spectral measurements were cut from the as-grown bulk crystals and two surfaces perpendicular to the a-axis were polished. The polarized absorption spectra were measured with the UH4150 ultraviolet visible near-infrared spectrophotometer produced by Hitachi, Tokyo, Japan, and the measurement range is 850–1100 nm. The polarized fluorescence spectra and fluorescence decay curves were obtained by the FLS1000 fluorescence spectrometer (Edinburgh, Livingston, UK) under the excitation of 905 nm light source. The cryogenic environment was achieved using a cryostat (model SU 12) with helium closed-circulation flow produced by Oxford Instruments Ltd. (Raleigh, NC, USA). The test was conducted at room temperature and low temperature.

3. Results and Discussion

3.1. Structure Measurement

Figure 2 shows the XRD pattern of the $\text{Yb:CaY}_{0.85}\text{Lu}_{0.05}\text{Gd}_{0.05}\text{AlO}_4$ crystal and the XRD standard card of CaYAlO_4 . It can be seen from the figure that the diffraction peak of the 5 at.% Yb:CALYGLO crystal with doping concentration is basically consistent with that of the PDF#81-0472 standard card. This indicates that after Lu^{3+} , Ga^{3+} , and Yb^{3+} are doped to replace the lattice position of Y^{3+} , the lattice structure of CaYAlO_4 has not changed significantly, and it is still a tetragonal system with a space group of $I4/mmm$.

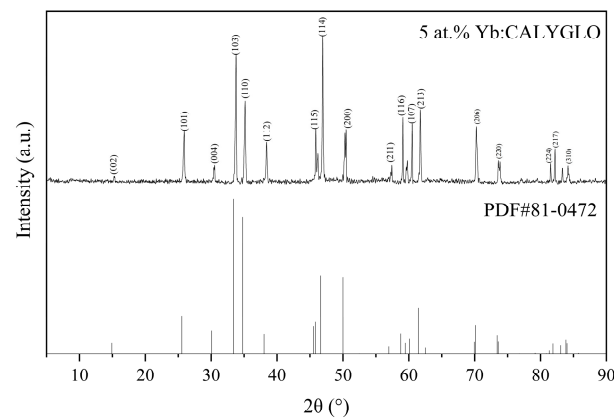


Figure 2. X-ray diffraction spectra of 5 at.% Yb:CALYGLO crystal and standard card of CALYO.

Using Jade software 4.6.0 (Jade Software Corporation, San Jose, CA, USA) to calculate, in the standard card, the lattice constant of CALYO crystal $a = b = 0.3645$ nm, $c = 1.1874$ nm, and the cell volume $V = 0.1577$ nm³. 5 at.% $\text{Yb:CaY}_{0.85}\text{Lu}_{0.05}\text{Gd}_{0.05}\text{AlO}_4$ crystal lattice constant $a = b = 0.3623$ nm, $c = 1.1550$ nm, cell volume $V = 0.1516$ nm³. It can be seen from the comparison that the lattice constants after Yb^{3+} , Lu^{3+} , and Gd^{3+} replace the lattice sites of Y^{3+} are slightly smaller than those of pure crystals. At the same time, the diffraction peak of the $\text{Yb:CaY}_{0.85}\text{Lu}_{0.05}\text{Gd}_{0.05}\text{AlO}_4$ crystal shifts to the right compared with that of the standard card. Due to the radius of Yb^{3+} (0.086 nm), the radius of Gd^{3+} (0.105 nm) and the radius of Lu^{3+} (0.085 nm) are smaller than the radius of Y^{3+} (0.111 nm); the introduction of Yb^{3+} , Lu^{3+} , and Gd^{3+} resulted in slight changes in crystal cell parameters.

3.2. Optical Absorption Spectra

The absorption cross-section is calculated by Equation (3):

$$\sigma_{abs}(\lambda) = \frac{\ln 10}{L \cdot N_0} \cdot OD(\lambda) \quad (3)$$

where L is the sample thickness, $OD(\lambda)$ is the optical density at the test wavelength, and N_0 is the concentration of doped ions.

Figure 3a shows the polarization absorption spectra of the Yb:CALYGLO crystal in the wavelength range of 850–1100 nm at low temperature. The main absorption peak at 980.4 nm is a zero phonon line, which corresponds to the transition of Yb³⁺ ions from the ²F_{7/2} ground state to the ²F_{5/2} excited state. The peaks of low-temperature absorption in both polarization directions are at 980.4 nm, and the absorption cross-sections peaks in the σ and π polarization directions are 3.98×10^{-20} and 9.38×10^{-20} cm², respectively. For zero phonon lines near 980 nm, as the temperature decreases, the peak becomes sharper and easier to distinguish. At lower temperatures, the phonon transitions corresponding to the peak patterns become clearer. This feature was also found in Yb:YAG crystals [28].

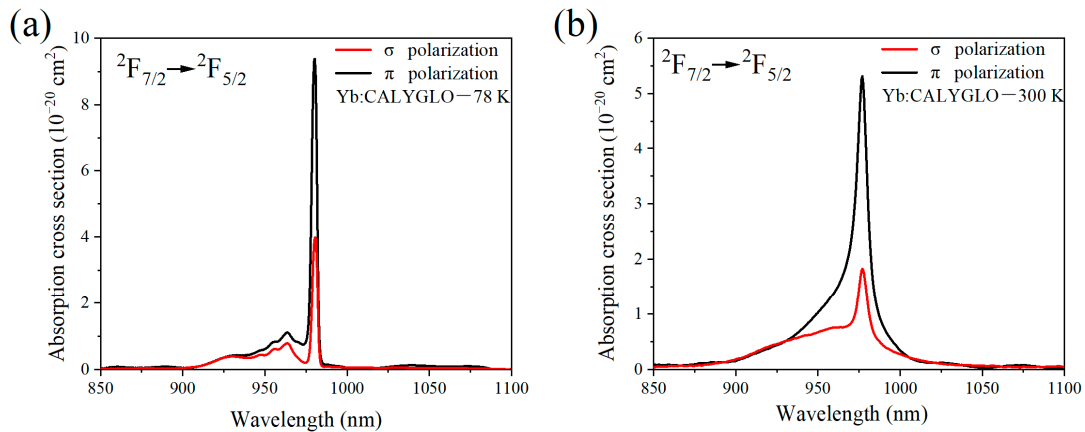


Figure 3. The polarized absorption cross-section of 5 at.% Yb:CALYGLO at low temperature (a) and room temperature (b).

Figure 3b shows the polarization absorption spectra of the Yb:CALYGLO crystal at room temperature. The absorption spectrum has strong polarization, which is caused by the anisotropy of the crystal. According to the test results, the absorption cross-section in the π polarization direction is mostly larger than the absorption cross-section in the σ polarization direction. The absorption cross-sections peaks in the σ and π polarization directions are 1.83×10^{-20} and 5.32×10^{-20} cm², respectively. This absorption cross-section is larger than that of Yb:CALYO [29], and FWHM for σ and π polarizations are 9.59 and 10.08 nm. The Yb:CALYGLO crystal has a large full width at half maxima (FWHM), indicating that the Yb:CALYGLO crystal can be pumped more efficiently with LD to achieve high conversion efficiency.

3.3. Emission Spectra

Under 905 nm excitation, the polarized fluorescence intensity of the Yb:CALYGLO crystal was measured in the range of 950–1150 nm. According to the measured fluorescence intensity, the stimulated emission cross-section of Yb³⁺ ions in the CALYGLO crystal is calculated through the Füchtbauer–Ladenburg (F-L) formula [30].

$$\sigma_q^{\text{em}}(\lambda) = \frac{\lambda^5 I_q(\lambda)}{8\pi c n^2 \tau_r \int \lambda I_q(\lambda) d\lambda} \quad (4)$$

where λ is the wavelength, n is the refractive index, $I(\lambda)$ is the relative emission intensity, and τ_r is the radiative lifetime. The radiative lifetime of the Yb:CALYGLO crystal was calculated to be 529 μ s. The radiative lifetime of the Yb:CALYGLO crystal, calculated to be 529 μ s, is determined from the emission cross-section using the reciprocity method (RM) [8].

Figure 4a shows the stimulated emission cross-sections of different polarizations, mainly focusing on the emission bands centered on 950–1150 nm, corresponding to the ²F_{5/2} → ²F_{7/2} emission bands. The main emission spectra peaks in the low-temperature are

observed at 981 nm, 997.5 nm, 1020 nm, and 1045 nm, corresponding to the Stark splitting of Yb^{3+} ions from excited state to ground state in CALYGLO crystals. The low-temperature peak emission cross-sections for σ polarization are $0.51 \times 10^{-20} \text{ cm}^2$, $0.83 \times 10^{-20} \text{ cm}^2$, $1.01 \times 10^{-20} \text{ cm}^2$, and $1.07 \times 10^{-20} \text{ cm}^2$, and the peak emission cross-sections for π polarization are $0.50 \times 10^{-20} \text{ cm}^2$, $0.89 \times 10^{-20} \text{ cm}^2$, $0.94 \times 10^{-20} \text{ cm}^2$, and $1.00 \times 10^{-20} \text{ cm}^2$. The peak patterns of low-temperature emission are basically the same in both polarization directions.

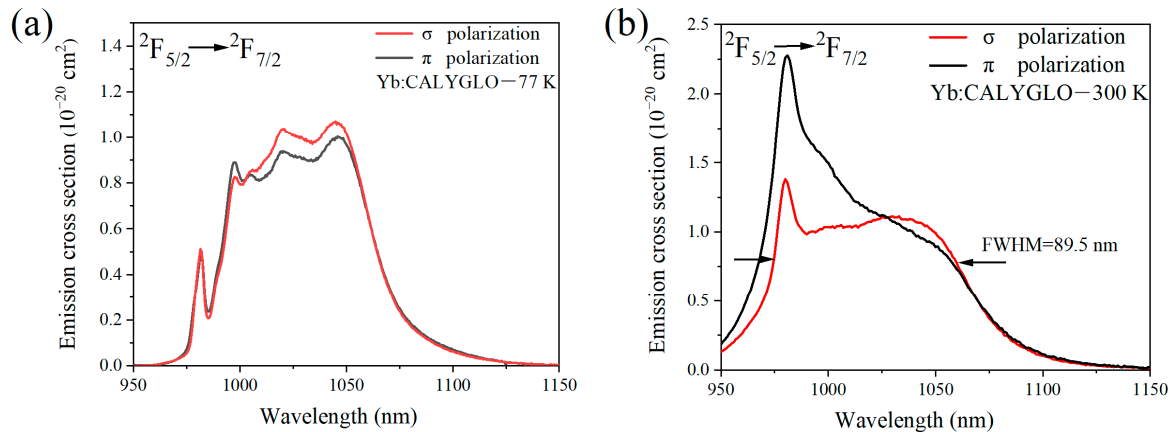


Figure 4. The polarized emission spectra of 5 at.% Yb:CALYGLO at low temperature (a) and room temperature (b).

Figure 4b shows the stimulated polarization emission cross-sections of the Yb:CALYGLO crystal at room temperature. The polarization of the emission spectrum is the same as that of the absorption spectrum. From the figure, we can see that the emission cross-section in the π polarization direction is larger than the emission cross-section in the σ polarization direction. The peak emission cross-section for σ polarization at 980 nm is $1.38 \times 10^{-20} \text{ cm}^2$, and the peak emission cross-section for π polarization at 981 nm is $2.28 \times 10^{-20} \text{ cm}^2$. Under σ polarization, the peak emission cross-section of Yb:CALYGLO is slightly larger than Yb:CALYO ($1.38 \times 10^{-20} \text{ cm}^2$) [31], and the emission spectrum of Yb:CALYGLO is significantly broadened. In the σ polarization direction, the full width at half maximum (FWHM) of the emission spectrum of Yb:CALYGLO is 89.5 nm. The FWHM of the stimulated emission cross-section of Yb:CALYGLO in σ polarization is larger than that of the Yb:CaYAlO₄ crystal (76 nm for σ polarization [31]), Yb:CaGdAlO₄ crystal (80 nm for σ polarization [32]), and Yb:SrLaAlO₄ (89 nm for σ polarization [33]). The broad and smooth emission spectrum of the Yb:CALYGLO crystal is conducive to the realization of mode-locked ultrashort pulse laser output.

Figure 5 illustrates the energy level scheme of Yb^{3+} ions in CALYGLO, highlighting the transitions responsible for absorption and emission. The Stark splitting of the ground and excited states of Yb^{3+} ions in CALYGLO crystals is to be determined through polarization absorption and fluorescence spectroscopy under low-temperature conditions. The calculated partition functions $Z_{1(2)}$ are indicated by the arrows. The ratio Z_1/Z_2 is found to be 1.16, which closely aligns with the values reported in recent studies on Yb^{3+} -doped CaLnAlO₄ crystals [34]. Additionally, the ground-state exhibits a total splitting of 624 cm^{-1} , making it highly suitable for wavelength tunable laser operation.

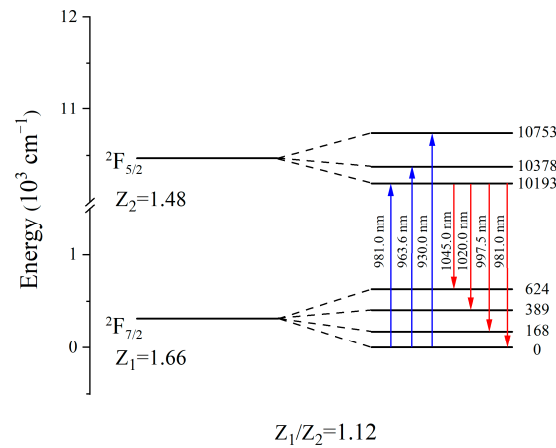


Figure 5. Scheme of the stark splitting of the Yb^{3+} multiplets in the CALYGLO crystal.

3.4. Fluorescence Lifetime

Figure 6 shows the fluorescence decay curves of ${}^2\text{F}_{5/2} \rightarrow {}^2\text{F}_{7/2}$ levels in the Yb:CALYGLO crystal under excitation at 905 nm at low temperature and room temperature. The fitting equation is as follows:

$$y = y_0 + Ae^{-x/t} \quad (5)$$

where Y is the fitted equation; x , y , and A are the constants of the fitted equation; and t is the fluorescence lifetime obtained after fitting. In Figure 6a, the low-temperature fluorescence lifetime of the Yb:CALYGLO crystal, after single exponential fitting, is measured to be 873 μs . The measured fluorescence lifetime is found to be larger than the radiative lifetime due to the presence of the radiation trapping effect in Yb^{3+} -doped materials. This effect occurs because the fluorescence spectrum and absorption spectrum of Yb^{3+} overlap, leading to re-absorption of photons emitted from the excited state energy level by the ground state energy level. This self-absorption effect not only alters the shape of the fluorescence spectrum but also facilitates energy transfer and migration over long distances, resulting in fluorescence capture. As a result, the fluorescence lifetime measured at room temperature is longer than that measured at low temperature and the actual radiative lifetime. This is consistent with the reported situation of Yb:YAG [35].

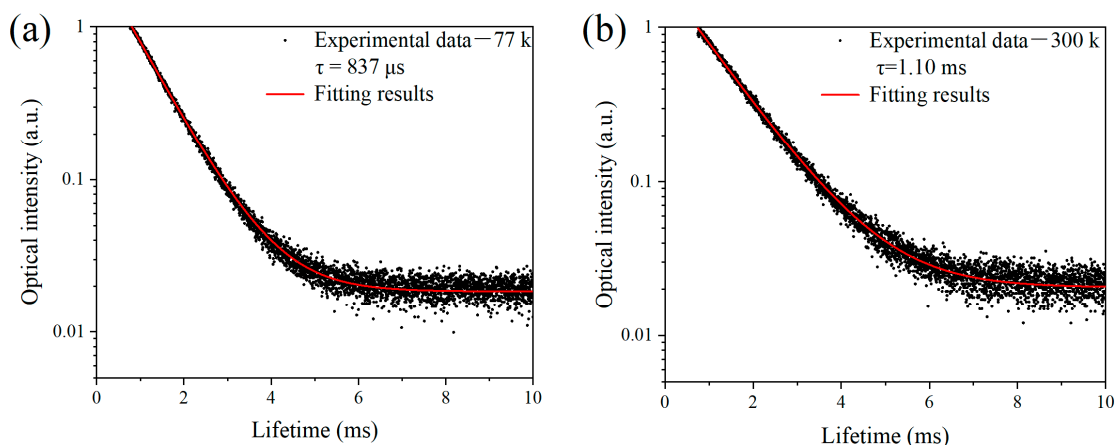


Figure 6. The fluorescence decay curve of the ${}^2\text{F}_{5/2}$ manifold of Yb:CALYGLO at low temperature (a) and room temperature (b).

In Figure 6b, the room temperature fluorescence lifetime of the Yb:CALYGLO crystal, after single exponential fitting, is measured to be 1.10 ms. This value is longer than the fluorescence lifetime of Yb^{3+} in the CaYAlO_4 crystal [31]. Meanwhile, it is longer than the fluorescence lifetime of Yb:CaGdAlO₄ (420 μs [32]), Yb:SrLaAlO₄ (630 μs [33]), and

Yb:YAG (950 μs [36]). The longer fluorescence lifetime of the Yb:CALYGLO crystal allows for efficient energy storage and laser output.

3.5. The Gain Cross-Section

The calculated polarization gain cross-sections for two polarizations (σ and π) with different β values are shown in Figure 7. For the quasi three-level laser systems, the gain cross-section can be used to predict the potential gain bandwidth for tunable or mode-locked (ML) operation, which is an important parameter directly related to laser applications. The relative strength of the gain cross-section can be obtained from Equation (6) [37]:

$$\sigma_g^\alpha(\lambda) = \beta\sigma_{em}^\alpha(\lambda) - (1 - \beta)\sigma_{abs}^\alpha(\lambda) \quad (6)$$

where β stands for the Yb³⁺ ions population inversion ratio of the laser upper level, which is the ratio of the inverted ions to the total Yb³⁺ ion density. σ_{abs} is the measured absorption cross-section, and σ_{em} is the calculated emission cross-section.

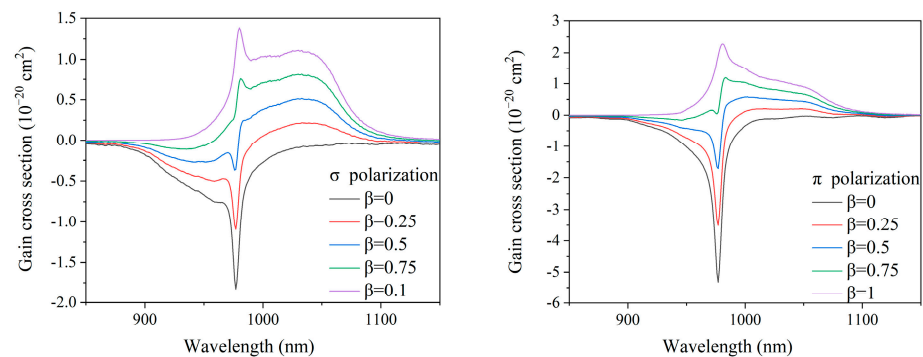


Figure 7. The polarized gain cross-section σ_g of 5 at.% Yb:CALYGLO.

When the β is 0.25, the gain cross-section is positive in the range of 995–1104 nm (σ polarization), and the peak gain cross-section at 1033 nm is $0.22 \times 10^{-20} \text{ cm}^2$. In the π polarization, the gain cross-section is positive in the range of 995–1092 nm, and the peak gain cross-section at 1016 nm is $0.21 \times 10^{-20} \text{ cm}^2$. For a population inversion level of 50%, the gain cross-section in the σ polarization direction becomes positive starting from 980 nm, and the gain cross-section in the π polarization direction becomes positive starting from 982 nm. The wavelength edge reaches 965 nm when the population inversion ratio is 0.75. The peak gain cross-section for this level is $0.81 \times 10^{-20} \text{ cm}^2$ at 1033 nm (σ polarization). The absorption cross-section spectrum and emission cross-section spectrum correspond to $\beta = 0$ and $\beta = 1$, respectively. Under different β values, the gain cross-section and bandwidth in the σ polarization direction are larger than the gain cross-section and bandwidth in the π polarization direction. For a 5 at.% Yb:CALYGLO crystal, the full width at half maximum (FWHM) of the gain band is approximately 90.0 nm ($\beta = 0.75$) for σ polarization and 80.0 nm ($\beta = 0.5$) for π polarization. Furthermore, the results demonstrate that the Yb:CALYGLO crystal exhibits broad and remarkably flat gain spectra for both polarizations. As a result, the Yb:CALYGLO crystal holds significant potential in the generation of tunable lasers and ultrafast mode-locked pulses.

3.6. Comparison with Other Host Material

Table 2 presents a comparison of several important spectral parameters between the Yb:CALYGLO crystal and other Yb³⁺-doped laser crystals. Notably, the Yb:CALYGLO crystal exhibits a larger absorption cross-section, making it highly suitable for LD pumping. Furthermore, this crystal demonstrates a significant advantage over other matrix materials in terms of possessing a large emission cross-section and broad fluorescence spectra. As a result, the Yb:CALYGLO crystal offers a substantial and wide gain cross-section, thereby

facilitating laser operation. These findings strongly suggest that the Yb:CALYGLO crystal fiber holds great potential as a laser gain medium operating at around 1 μm .

Table 2. Comparison of spectral parameters with other Yb³⁺ ion laser crystals.

Crystals	Yb:CALYGLO	Yb:CaYAlO ₄	Yb:CaGdAlO ₄	Yb:SrLaAlO ₄	Yb:YAG	Yb:KY(WO ₄) ₂
Absorption peak wavelength (nm)	977	979	979	980	968	981
Absorption cross-section (10 ⁻²⁰ cm ²)	1.83 (σ)	1.71 (σ)	1.03 (σ)	0.72 (σ)	0.94	1.67 (X)
	5.32 (π)	5.07 (π)	2.65 (π)	1.37 (π)		0.78 (Y)
Absorption cross-section bandwidth (FWHM) (nm)	9.59 (σ)	15 (σ)	29 (σ)	13 (σ)	3	8 (X)
	10.08 (π)	11 (π)	17 (π)	24 (π)		6 (Y)
						7 (Z)
Emission peak wavelength (nm)	980	980	980	980.2 (σ)	1030	1025
Emission cross-section (10 ⁻²⁰ cm ²)	1.38 (σ)	1.07 (σ)	1.43 (σ)	0.8 (σ)	2.2	1.82 (X)
	2.28 (π)	3.12 (π)	2.23 (π)			
Emission cross-section bandwidth (FWHM) (nm)	89.50 (σ)	76 (σ)	76 (σ)	89 (σ)	10	15 (X)
	50.26 (π)		23 (π)			
Fluorescence lifetime (μs)	1105	426	420	630	950	600
References	This work	[29,31]	[32,38]	[33]	[36]	[39,40]

3.7. Continuous-Wave Laser

The Yb:CALYGLO crystal used in this study had a Yb³⁺ doping concentration of $4.34 \times 10^{20} \text{ cm}^{-2}$, which corresponds to 3.4 at.%. The crystal was cut along the crystallographic *a*-axis into cubic samples with dimensions of 3 mm in length and width and 5 mm in thickness. The *a*-cut crystal we use corresponds to the σ polarization. In order to remove the heat generated during laser operation, the crystal was wrapped in indium foil and installed in a copper block heat sink, maintained at a temperature of about 20.0 °C through circulating water. The laser performance of Yb:CALYGLO was investigated using a LD-pumped continuous-wave laser in a plano-plano resonator configuration. The collimator f_1 is about 50 mm, and the focusing mirror f_2 is about 100 mm. The experimental set-up is illustrated in Figure 8. The pump source employed was a fiber-coupled 976 nm InGaAs diode laser with a core diameter of approximately 105 μm and a numerical aperture of 0.22. To vary the output power, we used four different output couplers (OCs) with transmissions of 5%, 10%, 15%, and 20% at 1055 nm.

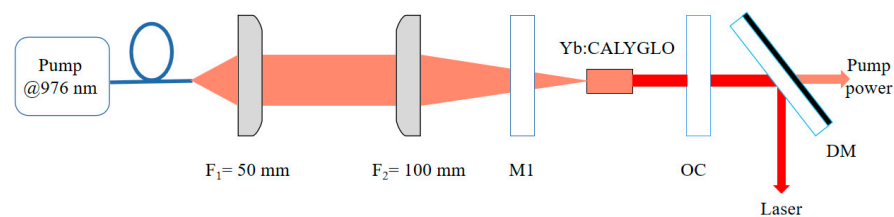


Figure 8. Experimental set up of the CW Yb:CALYGLO laser.

The relationship between the output power of a 5 at.% Yb:CALYGLO crystal and the pump power is shown in Figure 9a. When the transmittance of the output coupling mirror is 5%, the output power begins at 0.2 W when the pump power reaches 5.2 W. The output power reaches its maximum at a pump power of 23.2 W, reaching 6.6 W. The output power starts at 0.2 W when the pump power is 8.0 W. At a pump power of 31.9 W, the maximum output power is achieved at 10.8 W with a slope efficiency of 46%. When the transmittance of the output coupling mirror is 20%, the output power begins at 0.1 W when the pump power is 8.8 W. At a pump power of 32.8 W, the maximum output power is achieved, reaching 9.8 W.

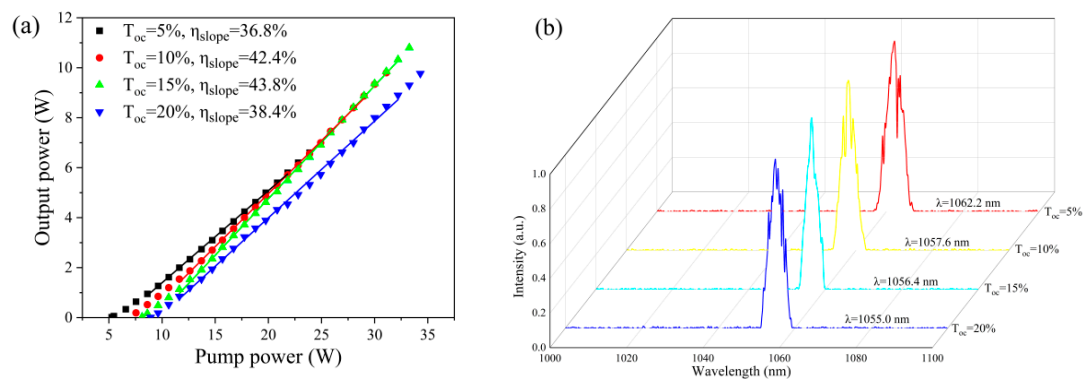


Figure 9. CW laser performance of an a-cut 5 at.% Yb:CALYGLO crystal: (a) absorbed-output dependences, η : slope efficiency; (b) typical spectra of laser emission.

The output laser spectrum is illustrated in Figure 9b. For transmissivity values of 5%, 10%, 15%, and 20% for the output coupling mirror, the central wavelengths are 1062.2 nm, 1057.6 nm, 1056.4 nm, and 1055.0 nm, respectively. This blue-shift of the laser wavelength as the output coupling increases is a characteristic behavior observed in quasi-three-level Yb^{3+} lasers due to inherent reabsorption at the laser wavelength.

4. Conclusions

Using the Czochralski method, $\text{Yb:CaY}_{0.85}\text{Lu}_{0.05}\text{Gd}_{0.05}\text{AlO}_4$ crystals were successfully grown. In the host lattice of $\text{CaY}_{0.85}\text{Lu}_{0.05}\text{Gd}_{0.05}\text{AlO}_4$, the segregation coefficient of Yb^{3+} is 0.65, and the actual doping concentration of Yb^{3+} ions is only 3.4 at.%. The polarized absorption spectra, fluorescence spectra, and fluorescence lifetimes were tested and analyzed at both low and room temperatures. At room temperature, the highest absorption peak occurred at 977 nm, with absorption cross-sections of $1.83 \times 10^{-20} \text{ cm}^2$ for σ polarization and $5.32 \times 10^{-20} \text{ cm}^2$ for π polarization, respectively. The stimulated emission cross-section for the peak at 980 nm, corresponding to the transition ${}^2F_{5/2} \rightarrow {}^2F_{7/2}$, was calculated to be $1.38 \times 10^{-20} \text{ cm}^2$ for σ polarization and $2.28 \times 10^{-20} \text{ cm}^2$ for π polarization, with FWHM values of 50.26 nm and 89.50 nm, respectively. The Stark splitting of the ground and excited states of Yb^{3+} ions in CALYGLO crystals through polarized absorption and fluorescence spectra measurements were determined under low-temperature conditions, and the partition function of the crystal was calculated. The fluorescence lifetimes of a 5 at.% Yb:CALYGLO crystal was tested and calculated at low and room temperatures, resulting in 873 μs and 1.10 ms, respectively. The polarization gain cross-sections were calculated for different β values. The main spectroscopic parameters of $\text{Yb:CaY}_{0.85}\text{Lu}_{0.05}\text{Gd}_{0.05}\text{AlO}_4$ are comparable to those of Yb:CaYAlO_4 , but the spectrum has been broadened. In the continuous laser experiment, the crystal achieved a laser output of 10.8 W with an oblique efficiency of 43.8%. These experimental results indicate that Lu^{3+} and Gd^{3+} can be used to replace part of the Y^{3+} lattice, broadening the crystal's spectrum and making it a potential ultrashort pulse laser crystal gain medium.

Author Contributions: Conceptualization, X.X.; Methodology, J.L., P.C. and X.X.; Validation, K.L.; Formal analysis, Z.W., P.C., J.M., X.X. and K.L.; Investigation, Z.W. and Y.W.; Resources, Z.W., P.L., X.X., Y.W., K.L. and J.X.; Data curation, Z.W., J.L., P.C., P.L. and J.M.; Writing—original draft, Z.W.; Writing—review & editing, J.L.; Visualization, P.L.; Project administration, J.X.; Funding acquisition, Y.W. All authors have read and agreed to the published version of the manuscript.

Funding: This work is partially supported by the National Natural Science Foundation of China (No. 61975071) and Education Department of Hunan Province (Grant No. 22A0476).

Data Availability Statement: The original contributions presented in the study are included in the article, further inquiries can be directed to the corresponding author.

Conflicts of Interest: The authors declare no conflict of interest.

References

1. Keller, U. Recent developments in compact ultrafast lasers. *Nature* **2003**, *424*, 831–838. [[CrossRef](#)]
2. Zhang, H.; Liu, X.; Li, Y.; Wu, W.; Gu, Y.; Zhang, T. Study on the mechanism of thrombus ablation in vitro by burst-mode femtosecond laser. *J. Biophotonics* **2022**, *15*, e202200197. [[CrossRef](#)]
3. Zhang, F.; Zhu, H.; Liu, J.; He, Y.; Jiang, D.; Tang, F.; Su, L. Tunable Yb: CaF₂-SrF₂ laser and femtosecond mode-locked performance based on semiconductor saturable absorber mirrors. *Appl. Opt.* **2016**, *55*, 8359–8362. [[CrossRef](#)] [[PubMed](#)]
4. Phillips, K.C.; Gandhi, H.H.; Mazur, E.; Sundaram, S.K. Ultrafast laser processing of materials: A review. *Adv. Opt. Photonics* **2015**, *7*, 684–712. [[CrossRef](#)]
5. Ahmmed, K.M.T.; Grambow, C.; Kietzig, A. Fabrication of Micro/Nano Structures on Metals by Femtosecond Laser Micromachining. *Micromachines* **2014**, *5*, 1219–1253. [[CrossRef](#)]
6. Kawata, S.; Sun, H.B.; Tanaka, T.; Takada, K. Finer features for functional microdevices. *Nature* **2001**, *412*, 697–698. [[CrossRef](#)] [[PubMed](#)]
7. Wang, W.; Wang, K.; Hao, W.; Zhang, T.; Liu, Y.; Yu, L.; Li, W. Preparation of Ti-based Yb-doped SnO₂-RuO₂ electrode and electrochemical oxidation treatment of coking wastewater. *J. Rare Earths* **2022**, *40*, 763–771. [[CrossRef](#)]
8. DeLoach, L.D.; Payne, S.A.; Chase, L.L.; Smith, L.K.; Kway, W.L.; Krupke, W.F. Evaluation of absorption and emission properties of Yb³⁺ doped crystals for laser applications. *IEEE J. Quantum Electron.* **1993**, *29*, 1179–1191. [[CrossRef](#)]
9. Zhang, Y.; Li, S.; Du, X.; Guo, J.; Gong, Q.; Tao, S.; Zhang, P.; Fang, Q.; Pan, S.; Zhao, C.; et al. Yb:GdScO₃ crystal for efficient ultrashort pulse lasers. *Opt. Lett.* **2021**, *46*, 3641–3644. [[CrossRef](#)]
10. Drs, J.; Fischer, J.; Modsching, N.; Labaye, F.; Wittwer, V.; Südmeyer, T. Sub-30-fs Yb:YAG thin-disk laser oscillator operating in the strongly self-phase modulation broadened regime. *Opt. Express* **2021**, *29*, 35929–35937. [[CrossRef](#)]
11. Seidel, M.; Pilat, J.; Lang, L.; Phillips, C.R.; Keller, U. Ultrafast Yb:YAG laser oscillator with gigahertz repetition rate. *Opt. Express* **2023**, *31*, 34313–34324. [[CrossRef](#)]
12. Ostapenko, H.; Feng, Y.; Lamour, T.; McCracken, R.; Mandel, O.; Weise, D.; Reid, D. Misalignment-free, Kerr-lens-modelocked Yb:Y₂O₃ 2.2-GHz oscillator, amplified by a semiconductor optical amplifier. *Opt. Express* **2023**, *31*, 3249–3257. [[CrossRef](#)]
13. Su, X.; Wang, Y.; Yin, Y.; Wang, M.; Zhang, B.; He, J.; Zhang, B. Sub-100-fs Kerr-lens mode-locked Yb:Lu₂O₃ laser with more than 60% optical efficiency. *Opt. Lett.* **2024**, *49*, 145–148. [[CrossRef](#)]
14. Kim, D.Y.; Park, B.J.; Lee, S.Y.; Yee, K.J. High-power 50 fs Kerr-lens mode-locked Yb:CALGO oscillator. *Opt. Laser Technol.* **2023**, *159*, 109019. [[CrossRef](#)]
15. Wang, H.; Pan, J.; Meng, Y.; Liu, Q.; Shen, Y. Advances of Yb:CALGO Laser Crystals. *Crystals* **2021**, *11*, 1131. [[CrossRef](#)]
16. Pajaczkowska, A.; Gloubokov, A. Synthesis, growth and characterization of tetragonal ABCO₄ crystals. *Prog. Cryst. Growth Charact. Mater.* **1998**, *36*, 123–162. [[CrossRef](#)]
17. Petit, P.O.; Petit, J.; Goldner, P.; Viana, B. Inhomogeneous broadening of optical transitions in Yb:CaYAlO₄. *Opt. Mater.* **2008**, *30*, 1093–1097. [[CrossRef](#)]
18. Sévillano, P.; Georges, P.; Druon, F.; Descamps, D.; Cormier, E. 32-fs Kerr-lens mode-locked Yb:CaGdAlO₄ oscillator optically pumped by a bright fiber laser. *Opt. Lett.* **2014**, *39*, 6001–6004. [[CrossRef](#)] [[PubMed](#)]
19. Pirzio, F.; Cafiso, S.D.D.D.; Kemnitzer, M.; Guandalini, A.; Kienle, F.; Veronesi, S.; Tonelli, M.; Au, J.A.D.; Agnesi, A. Sub-50-fs widely tunable Yb:CaYAlO₄ laser pumped by 400-mW single-mode fiber-coupled laser diode. *Opt. Express* **2015**, *23*, 9790–9795. [[CrossRef](#)] [[PubMed](#)]
20. Molteni, L.M.; Pirzio, F.; Manzoni, C.; Galzerano, G.; Laporta, P.; Agnesi, A. Few-optical-cycle pulse generation based on a non-linear fiber compressor pumped by a low-energy Yb:CALGO ultrafast laser. *Opt. Express* **2020**, *28*, 13714–13720. [[CrossRef](#)] [[PubMed](#)]
21. Agnesi, A.; Greborio, A.; Pirzio, F.; Reali, G.; Au, J.A.D.; Guandalini, A. 40-fs Yb³⁺:CaGdAlO₄ laser pumped by a single-mode 350-mW laser diode. *Opt. Express* **2012**, *20*, 10077–10082. [[CrossRef](#)]
22. Hu, Q.; Jia, Z.; Volpi, A.; Veronesi, S.; Tonelli, M.; Tao, X. Crystal growth and spectral broadening of a promising Yb:CaLu_xGd_{1-x}AlO₄ disordered crystal for ultrafast laser application. *CrystEngComm* **2017**, *19*, 1643–1647. [[CrossRef](#)]
23. Pan, Z.; Loiko, P.; Serres, J.M.; Kifle, E.; Yuan, H.; Dai, X.; Cai, H.; Wang, Y.; Zhao, Y.; Aguiló, M.; et al. “Mixed” Tm:Ca(Gd,Lu)AlO₄—A novel crystal for tunable and mode-locked 2 μm lasers. *Opt. Express* **2019**, *27*, 9987–9995. [[CrossRef](#)] [[PubMed](#)]
24. Beil, K.; Fredrich-Thornton, S.T.; Tellkamp, F.; Peters, R.; Kränkel, C.; Petermann, K.; Huber, G. Thermal and laser properties of Yb:LuAG for kW thin disk lasers. *Opt. Express* **2010**, *18*, 20712–20722. [[CrossRef](#)]
25. Pan, Z.; Loiko, P.; Slimi, S.; Yuan, H.; Wang, Y.; Zhao, Y.; Camy, P.; Dunina, E.; Kornienko, A.; Fomicheva, L.; et al. Tm,Ho:Ca(Gd,Lu)AlO₄ crystals: Crystal growth, structure refinement and Judd-Ofelt analysis. *J. Lumin.* **2022**, *246*, 118828. [[CrossRef](#)]
26. Chen, H.; Zhang, P.; Song, J.; Yin, H.; Hang, Y.; Yang, Q.; Li, Z.; Chen, Z. Spectral broadening of a mixed Nd: CYGA crystal with tunable laser operation beyond 1100 nm. *Opt. Express* **2022**, *30*, 21943–21951. [[CrossRef](#)]
27. Slimi, S.; Loiko, P.; Pan, M.; Lehoux, P.; Jambunathan, V.; Smrz, M.; Mocek, T.; Wang, Y.; Chen, W.; Petrov, V.; et al. Growth, Structure, Spectroscopy, and Laser Operation of a “Mixed” Yb:(Y,Lu)₃Al₅O₁₂ Garnet Crystal. *Crystals* **2023**, *13*, 1588. [[CrossRef](#)]
28. Brown, D.C.; Cone, R.L.; Sun, Y.C.; Equal, R.W. Yb:YAG absorption at ambient and LF cryogenic temperatures. *IEEE J. Sel. Top. Quant.* **2005**, *11*, 604–612. [[CrossRef](#)]

29. Li, D.; Xu, X.; Cheng, Y.; Cheng, S.; Zhou, D.; Wu, F.; Xia, C.; Xu, J.; Zhang, J. Crystal growth and spectroscopic properties of Yb:CaYAlO₄ single crystal. *J. Cryst. Growth* **2010**, *312*, 2117–2121. [[CrossRef](#)]
30. Hutchinson, J.A.; Verdun, H.R.; Chai, B.H.T.; Zandi, B.; Merkle, L.D. Spectroscopic evaluation of CaYAlO₄ doped with trivalent Er, Tm, Yb and Ho for eyesafe laser applications. *Opt. Mater.* **1994**, *3*, 287–306. [[CrossRef](#)]
31. Li, D.; Xu, X.; Zhu, H.; Chen, X.; Tan, W.; Zhang, J.; Tang, D.; Ma, J.; Wu, F.; Xia, C.; et al. Characterization of laser crystal Yb:CaYAlO₄. *J. Opt. Soc. Am. B* **2011**, *28*, 1650–1654. [[CrossRef](#)]
32. Zaouter, Y.; Didierjean, J.; Balembois, F.; Lucas-Leclin, G.; Druon, F.; Georges, P.; Petit, J.; Goldner, P.; Viana, B. 47-fs diode-pumped Yb³⁺:CaGdAlO₄ laser. *Opt. Lett.* **2006**, *31*, 119–121. [[CrossRef](#)]
33. Pan, Z.; Dai, X.; Lei, Y.; Cai, H.; Serres, J.M.; Aguiló, M.; Díaz, F.; Ma, J.; Tang, D.; Vilejshikova, E.; et al. Crystal growth and properties of the disordered crystal Yb:SrLaAlO₄: A promising candidate for high-power ultrashort pulse lasers. *CrystEngComm* **2018**, *20*, 3388–3395. [[CrossRef](#)]
34. Loiko, P.; Serres, J.M.; Mateos, X.; Xu, X.; Xu, J.; Jambunathan, V.; Navratil, P.; Lucianetti, A.; Mocek, T.; Zhang, X.; et al. Microchip Yb:CaLnAlO₄ lasers with up to 91% slope efficiency. *Opt. Lett.* **2017**, *42*, 2431–2434. [[CrossRef](#)]
35. Dong, J.; Bass, M.; Mao, Y.; Deng, P.; Gan, F. Dependence of the Yb³⁺ emission cross section and lifetime on temperature and concentration in yttrium aluminum garnet. *J. Opt. Soc. Am. B* **2003**, *20*, 1975–1979. [[CrossRef](#)]
36. Yang, P.; Deng, P.; Huang, G.; Wu, G.; Yin, Z. Spectroscopy Performances of Yb³⁺ doped YAG Crystal. *Spectrosc. Spect. Anal.* **2000**, *20*, 286–289.
37. Ohta, K.; Saito, H.; Obara, M. Spectroscopic characterization of Tm³⁺:YVO₄ crystal as an efficient diode pumped laser source near 2000 nm. *J. Appl. Phys.* **1993**, *73*, 3149–3152. [[CrossRef](#)]
38. Di, J.; Xu, X.; Xia, C.; Zheng, L.; Aka, G.; Yu, H.; Sai, Q.; Guo, X.; Zhu, L. Crystal growth, polarized spectra, and laser performance of Yb:CaGdAlO₄ crystal. *Laser Phys.* **2016**, *26*, 045803. [[CrossRef](#)]
39. Liu, H.; Nees, J.; Mourou, G. Diode-pumped Kerr-lens mode-locked Yb:KY(WO₄)₂ laser. *Opt. Lett.* **2001**, *26*, 1723–1725. [[CrossRef](#)] [[PubMed](#)]
40. Tang, L.; Lin, Z.; Zhang, L.; Wang, G. Phase diagram, growth and spectral characteristic of Yb³⁺:KY(WO₄)₂ crystal. *J. Cryst. Growth* **2005**, *282*, 376–382. [[CrossRef](#)]

Disclaimer/Publisher’s Note: The statements, opinions and data contained in all publications are solely those of the individual author(s) and contributor(s) and not of MDPI and/or the editor(s). MDPI and/or the editor(s) disclaim responsibility for any injury to people or property resulting from any ideas, methods, instructions or products referred to in the content.